Frontiers in Bioscience Landmark

Front. Biosci. (Landmark Ed) **2025**; 30(7): 40077
https://doi.org/10.31083/FBL40077

Original Research

Dual Role of Quercetin in Promoting Early Wound Healing via Inhibiting Inflammatory Factors and Attenuating Scar Formation by Suppressing Myofibroblast Differentiation

Dan Wu[1,†], Mengyuan Jiang[2,†], Jing Zhang[3,4,*]

[1]Facial Plastic and Reconstructive Surgery, Eye & ENT Hospital, Fudan University, 200031 Shanghai, China
[2]Department of Plastic & Reconstructive Surgery, Shanghai Ninth People's Hospital, Shanghai Jiao Tong University School of Medicine, 200011 Shanghai, China
[3]Eye Institute and Department of Ophthalmology, Eye & ENT Hospital, Fudan University, 200031 Shanghai, China
[4]NHC Key laboratory of Myopia and Related Eye Diseases; Key Laboratory of Myopia and Related Eye Diseases, Chinese Academy of Medical Sciences, 200031 Shanghai, China
*Correspondence: zhangjing_fdeent@hotmail.com (Jing Zhang)
[†]These authors contributed equally.
Academic Editor: Pedro Fonte
Submitted: 29 April 2025 Revised: 16 June 2025 Accepted: 7 July 2025 Published: 25 July 2025

Abstract

Background: Quercetin, a naturally occurring flavonoid, possesses anti-inflammatory properties and has emerged as a potential modulator of tissue repair. Impaired wound healing and pathological scarring are often driven by excessive inflammation and dysregulated myofibroblast differentiation. Current therapeutic approaches, however, frequently fall short in simultaneously addressing these intertwined challenges. This study investigates whether quercetin can provide a bifunctional therapeutic advantage by promoting early wound closure through inflammation resolution and suppressing scar formation via the inhibition of myofibroblast differentiation. **Methods**: A murine excisional wound model was employed to evaluate quercetin's effects *in vivo*. Mice (C57BL/6, n = 8/group) received daily topical applications of 1% quercetin. Wound closure kinetics were meticulously quantified using planimetry. To assess molecular and cellular changes, protein levels (CASPASE-1, interleukin-1 beta (IL-1β), alpha-smooth muscle actin (α-SMA)) and collagen III/I ratios were determined through multiplex qPCR, RNA sequencing, western blot analysis, and histomorphometry. For *in vitro* investigations, human dermal BJ fibroblasts were treated with transforming growth factor beta 1 (TGF-β1) (10 ng/mL) $\pm$ quercetin (5–50 µM) to assess myofibroblast differentiation markers (α-SMA, collagen I) via immunofluorescence, western blot, and qPCR. **Results**: Quercetin significantly accelerated wound closure *in vivo*. The acceleration was accompanied by a reduction in the expression of IL-1β and CASPASE-1. RNA sequencing data revealed that quercetin's anti-inflammatory effects in early wound healing involve the modulation of inflammasome complexes, including NLRP3, as well as inflammasome-mediated signaling pathways. Furthermore, treated wounds exhibited increased collagen III/I ratios relative to control groups ($p < 0.05$), indicative of a more regenerative matrix remodeling process. *In vitro*, experiments demonstrated that quercetin suppressed TGF-β1-induced myofibroblast differentiation, evidenced by decreased α-SMA expression ($p < 0.05$) and reduced collagen I synthesis. Notably, quercetin exhibited cell type-specific effects: while suppressing BJ fibroblast migration (scratch assay), it enhanced keratinocyte proliferation. This unique duality prevents aberrant myofibroblast recruitment without compromising essential epithelial coverage—a critical balance for minimizing scar formation. **Conclusions**: Quercetin exhibits a compelling dual therapeutic role in wound healing: resolving inflammation to expedite early wound healing and inhibiting TGF-β-driven myofibroblast differentiation to attenuate scarring. By harmonizing these actions, quercetin addresses both phases of repair, positioning it as a promising candidate for scar-free wound therapy. Further efforts should focus on optimizing its bioavailability to enhance clinical translation.

Keywords: quercetin; wound healing; cicatrix; myofibroblasts; transforming growth factor beta; anti-inflammatory agents

1. Introduction

Cutaneous wound repair involves tightly regulated phases—hemostasis, inflammation, proliferation, and remodeling [1]. Initiated immediately upon injury, hemostasis occurs through vasoconstriction and platelet aggregation to form a clot, controlling bleeding and establishing a provisional matrix [2]. This matrix serves as a scaffold for subsequent cell migration while releasing growth factors (e.g., platelet-derived growth factor, PDGF) to initiate the inflammatory response [3]. In the early stages of inflammation (24–48 hours), neutrophils migrate to the wound, clearing pathogens and necrotic tissue [4]. In the later stages (2 to several days), macrophages release cytokines (such as tumor necrosis factor-alpha (TNF-α) and interleukin-6 (IL-6)) to coordinate immune response [5]. Strict inflammation regulation is crucial, as excessive or prolonged inflammation can lead to chronic wounds. In the proliferation stage, the body reconstructs tissue structure and function, cover-

ing the surface of wounds, mainly involving endothelial cell angiogenesis [6], re-epithelialization of keratinocytes [7], and promotion of fibroblast activation and angiogenesis by TGF-β, vascular endothelial growth factor (VEGF), and other factors [8]. During the remodeling stage, collagen fibers recombine with type III collagen, which is degraded and replaced with stronger type I collagen. The degree of cross-linking increases, and scar tissue matures [9].

Disruptions to this delicate balance, such as prolonged inflammation or persistent myofibroblast activation, often lead to impaired healing [10] and pathological scarring [11]. Current therapies, like corticosteroids [12] or TGF-β inhibitors [13] often compromise early healing while targeting fibrosis [14]. This highlights an urgent need for agents that can precisely regulate TGF-β signaling throughout the healing timeline.

Quercetin, a natural flavonoid compound widely present in the plant kingdom, with a chemical structure of 3,3′, 4′, 5,7-pentahydroxyflavone. It has significant antioxidant, anti-inflammatory, and immune regulatory functions [15]. Historically, quercetin rich herbs, such as mulberry leaves [16] and locust flowers, have been used in traditional Chinese medicine to treat inflammatory conditions and promote tissue repair, noted for their ability to "clear heat and detoxify, promote muscle growth, and reduce ulcers". Modern pharmacological research further confirms that quercetin inhibits inflammatory responses by regulating multiple signaling pathways such as NF-κB and MAPK, and reduces oxidative stress damage by activating antioxidant enzymes such as Superoxide Dismutase (SOD) and Glutathione Peroxidase (GSH Px) [17–20]. These characteristics position quercetin as a promising candidate molecule for skin wound treatment.

In addition to its strong potential to promote healing, quercetin also possesses properties that prevent fibrosis. Emerging evidence suggests quercetin can modulate TGF-β signaling, a key regulator of fibrosis [21–23]. For instance, in a bleomycin-induced pulmonary fibrosis mice model, quercetin treatment (50 mg/kg/day) group led to a 45% decrease in lung tissue hydroxyproline content and a 70% improvement in pathological scores [24]. Other studies, such as that done by Geng *et al.* [25] have found that quercetin could alleviate pulmonary fibrosis by regulating macrophage polarity and macrophage-to-myofibroblast transition, specifically in the inhibition of the TGF-β-Smad2/3 signaling pathway. In addition, quercetin has been observed to suppress fibrosis in nonalcoholic steatohepatitis, by impacting TGF-β and collagen type I alpha (COL1A) [26]. Despite this compelling evidence, quercetin's dual role in coordinating early healing and late-stage anti-fibrotic effects remains underexplored. We hypothesize that quercetin accelerates inflammation resolution to promote healing while simultaneously blocking myofibroblast trans-differentiation to prevent scarring.

2. Materials and Methods

2.1 Murine Excisional Wound Model and Scar Analysis

2.1.1 Animal Ethics and Housing

All procedures were approved by the Animal Ethics Committee of the Eye & ENT Hospital of Fudan University (Shanghai, China, Ethics number: 2020096) and followed the protocol from the National Institutes of Health Guide for the Care and Use of Laboratory Animals (NIH Publications No. 8023, revised 1978). Male BALB/c mice (8–10 weeks, 22–25 g, purchased from Huachuang Xinnuo Pharmaceutical Technology Co., Ltd., Shanghai, China) were housed under standard conditions (12-h light/dark cycle, 22 °C, 50% humidity) with free access to food and water.

2.1.2 Establishment of a Murine Dorsal Full-Thickness Excisional Skin Wound Model

Anesthesia: Mice were anesthetized via intraperitoneal injection (i.p.). A combination of ketamine hydrochloride and xylazine hydrochloride was used as the anesthetic agent. The anesthetic dosage was precisely set at ketamine hydrochloride (100 mg/kg, CAS 1867-66-9, Sigma-Aldrich Corporation, Burlington, MA, USA) and xylazine hydrochloride (10 mg/kg, CAS 23076-35-9, Yeasen Biotechnology Co., Ltd., Shanghai, China). Prior to injection, the calculated doses of ketamine and xylazine were mixed thoroughly under sterile conditions.

Following injection, mice were placed on warm, clean bedding and monitored closely until the desired anesthetic depth was achieved. Assessment of Anesthetic Depth: Adequate surgical anesthesia (loss of consciousness and nociception) was confirmed by the absence of a pedal withdrawal reflex (elicited by gentle toe pinch) and observation of stable, regular respiratory patterns. Surgical procedures commenced only upon confirmation of sufficient anesthesia.

Preoperative Preparation: Once an appropriate anesthetic plane was confirmed, mice were positioned in ventral recumbency on a sterile surgical platform. The dorsal fur over the intended surgical site (typically the interscapular or lumbar region) was carefully removed using electric clippers or depilatory cream, creating a sufficiently large hair-free area extending well beyond the planned wound margins. The shaved area was aseptically prepared by scrubbing with sterile gauze or cotton swabs saturated with 70% (v/v) ethanol solution, covering an area significantly larger than the surgical field. The skin was allowed to air dry completely.

Wound Creation: Under strict aseptic technique (utilizing sterile gloves and instruments), an autoclavable or disposable sterile skin biopsy punch was employed. Applied perpendicularly with steady pressure to the prepared dorsal skin, the punch was used to create a wound penetrating the full thickness of the skin (epidermis, dermis, and subcutaneous tissue). A single, circular full-thickness excisional wound with a precise diameter of 8 mm was gener-

ated. The excised skin disc was carefully removed from the punch, ensuring clean, well-defined wound edges without residual flaps or excessive crush injury. Minor bleeding, if present, was controlled by applying gentle pressure with sterile cotton-tipped applicators or gauze, avoiding undue trauma to the wound margins [27].

Postoperative Care: Immediately following wound creation, provision of postoperative analgesia was implemented. This consisted of either subcutaneous infiltration of a long-acting local anesthetic (e.g., 0.25% bupivacaine) around the wound perimeter or systemic administration of an analgesic agent (e.g., buprenorphine or butorphanol), as required by the approved protocol (This step is critical for animal welfare and an ethical requirement). Mice were transferred to individual, pre-warmed (~37 °C) recovery cages placed on a heating pad or under a warming lamp. Animals were monitored continuously until full recovery from anesthesia (evidenced by spontaneous movement and return of righting reflex). Postoperative monitoring included assessment of behavior, activity, wound condition, and overall health status for a minimum of 24–48 hours. Analgesia was administered according to the predetermined schedule.

2.1.3 Splinting Method

To prevent wound contraction and mimic human healing, silicone rings (8 mm inner diameter) were fixed around the wounds using surgical glue (Vetbond, Cat no. 1469SB, 3M Company, Maplewood, MI, USA) and sutures (6-0 nylon, Vicryl, Ethicon Inc., Somerville, NJ, USA). Customized silicone rings (Shanghai Yeyu biomedical Technology Co., Ltd., Shanghai, China) were fixed with surgical glue and sutures to standardize wound healing.

2.1.4 Treatment Regimen: Mice Were Randomized Into 3 Three Groups

Control group: Topical application of 100 µL PBS dropwise to the wound of each mouse daily.

Quercetin group: Topical application of 1% quercetin (w/w, Cat no. HY-18085, Purity 99.80%, MedChemExpress LLC, Monmouth Junction, NJ, USA) applied daily.

Transforming Growth Factor Beta 1 (TGF-β) group: Topical application of 500 ng/kg TGF-β1 (Cat no. HY-P7117, MedChemExpress LLC) as a positive drug to promote wound healing daily [28].

2.1.5 Wound Closure Monitoring

Wound areas were photographed on days 0, 2, 6, 12, and 28 using a digital camera. Planimetry analysis (Image J software, version 1.54, National Institutes of Health, Bethesda, MD, USA) quantified wound areas. Two authors who were blinded to the group assignment conducted the independently measurement and the average was acquired.

2.1.6 Tissue Harvesting

On days 2 (inflammation phase), 5 (proliferative phase) and 28 (remodeling phase), mice were euthanized (CO_2 overdose). Wound tissues (including 2 mm surrounding skin) were excised, bisected, and either fixed in 4% paraformaldehyde (histology) or snap-frozen (molecular analysis).

2.2 Histopathological Section Detection

2.2.1 Hematoxylin and Eosin (H&E) Staining

Harvested wound tissues were fixed in 4% paraformaldehyde (PFA, Cat no. P0099-3L, Beyotime Biotechnology Co., Ltd., Shanghai, China) for 24 h at 4 °C, dehydrated through a graded ethanol series (70–100%), cleared in xylene, and embedded in paraffin. Then, paraffin blocks were cut into 5 µm-thick sections using a rotary microtome (Leica RM2235, Leica Camera AG, Wetzlar, Hesse, Germany). The Sections were deparaffinized in xylene (2 × 5 min) and rehydrated through graded ethanol (100–70%) to distilled water. Deparaffinized sections were then immersed in Harris hematoxylin (Cat no. HHS32, MilliporeSigma, Burlington, MA, USA) for 5 min, followed by rinsing in tap water. After that, the sections were dipped in 1% acid ethanol (1% HCl in 70% ethanol) for 5 s to remove excess stain, washed in 0.2% ammonia water for 1 min to neutralize acidity and stained with 0.5% eosin Y (Cat no. 318906, MilliporeSigma, Burlington, MA, USA) for 2 min. The slides were finally dehydrated through ethanol (70%–100%), cleared in xylene, and mounted with neutral balsam.

2.2.2 Masson's Trichrome Staining

Staining Protocol: The procedure for deparaffinization and hydration were performed as described for as Hematoxylin and Eosin (H&E) staining. The sections were stained with Weigert's iron hematoxylin (Cat no. HT1079, MilliporeSigma, Burlington, MA, USA) for 10 min. Then, the sections were rinsed in acid ethanol (1% HCl) for 5 sec and blued in ammonia water, then were immersed in Biebrich scarlet/acid fuchsin solution (Cat no. HT151, MilliporeSigma, Burlington, MA, USA) for 5 min to stain cytoplasm. Subsequently, the samples were treated with 1% phosphomolybdic acid (Cat. no. S0094, Beijing Biosynthesis Biotechnology Co., Ltd., Beijing, China) for 10 min to remove excess dye and stained with 2% aniline blue (Cat no. B8563, MilliporeSigma) for 5 min to highlight collagen fibers. Finally, the sections were washed in 1% acetic acid for 2 min, while the dehydration and mounting were performed as described in the protocol. All of the images were captured by a microscope (Axio, Carl Zeiss, Oberkochen, Baden-Württemberg, Germany) and analyzed by two authors who were blinded to the group assignment.

2.2.3 Immunohistochemistry (IHC) and Immunofluorescence (IF)

For IHC, deparaffinized sections were incubated in 10 mM citrate buffer (pH 6.0) at 95 °C for 20 min using a microwave. Treatment with 3% hydrogen peroxide subsequently occurred for 10 min to quench endogenous peroxidase, followed by 5% bovine serum albumin (BSA, Cat no. ST2249, Beyotime Biotechnology Co., Ltd., Shanghai, China) in PBS for 30 min to block nonspecific binding. Sections were incubated overnight at 4 °C with anti-Ki-67 antibody (1:200 dilution, Cat no. ab15580, Abcam Limited, Cambridge, Cambridgeshire, UK) diluted in PBS containing 1% BSA. Sections were then washed with PBS (3 $\times$ 5 min). They were incubated with HRP-conjugated goat anti-rabbit IgG (1:500, Cat no. 7074, Cell Signaling Technology, Inc., Danvers, MA, USA) for 1 h at RT and developed with 3,3′-diaminobenzidine (DAB, Cat no. RES2041D, MilliporeSigma, Burlington, MA, USA) for 3–5 min. The images were captured with microscope (Axio, Carl Zeiss, Oberkochen, Baden-Württemberg, Germany) and analyzed by two independent authors who were blinded to the group assisgnment.

In Immunofluorescence (IF), the sections were incubated with primary antibody with caspase-1 (1:1000, cat no. GB15383-100, Servicebio Inc, Wuhan, Hubei, China), Interleukin-1 beta (IL-1β) (1:1000, cat no. GB15113-100, Servicebio Inc, Wuhan, Hubei, China), collagen I (1:1000, cat no. GB11022-100, Servicebio Inc, Wuhan, China) and collage III (1:1000, cat no. GB111629-100, Servicebio Inc, Wuhan, Hubei, China) overnight at 4 °C after routine dehydration, embedding and sectioning. Then, the sections were washed and incubated with Alexa Fluor 488 or Cy3 -conjugated Goat Anti-Rabbit IgG (1:500, Cat no. GB25303 and Cat no. GB21303, Servicebio Inc, Wuhan, Hubei, China) for 1 hour. Immunofluorescence was observed using a fluorescence microscope (Axio, Carl Zeiss, Oberkochen, Baden-Württemberg, Germany).

2.3 Western Blot

The total protein from cells were lysed with pre-cooled radioimmunoprecipitation (RIPA, Cat no. P0013B, Beyotime Biotechnology Co., Ltd. Shanghai, China) buffer, containing protease inhibitor cocktail (Cat no. P9599, F. Hoffmann-La Roche AG, Basel-Stadt, Switzerland). Then, 30 µg of total protein was separated by SDS-PAGE (Cat no. LK301, Shanghai Epizyme Biomedical Technology Co., Ltd., Shanghai, China) and transferred onto polyvinylidene fluoride membrane (MilliporeSigma, MA, USA). After blocking with 5% non-fat milk for 1 h, membranes were respectively incubated with primary antibodies against Alpha-Smooth Muscle Actin (α-SMA) (1:1000, cat no. A7248, ABclonal Technology, Woburn, MA, USA), ASC/TMS1 (1:1000, cat no. A16672, ABclonal Technology, Woburn, MA, USA), IL-1β (1:1000, cat no. A25874, ABclonal Technology, Woburn, MA, USA) and Caspase-1 (1:1000, cat no. A25308, ABclonal Technology, Woburn, MA, USA) at 4 °C overnight. The β-actin (1:10,000, cat no. 20536-1-AP, Proteintech Group, Inc, Rosemont, IL, USA) or β-Tubulin (1:10,000, cat no. ABL1030, Abbkine Scientific Co., Ltd., Wuhan, Hubei, China) was served as internal control. Then, the corresponding secondary antibodies of HRP-conjugated Goat Anti-Mouse IgG (1:2000, cat no. SA00001-1, Proteintech Group, Inc, Rosemont, IL, USA) or HRP-conjugated Goat Anti-Rabbit IgG (1:2000, cat no. SA00001-2, Proteintech Group, Inc, Rosemont, IL, USA) were added and incubated for 1 h at RT. The signals were visualized and the band intensities were quantified by densitometry using ImageJ Software version 1.6 (National Institutes of Health, Bethesda, MD, USA).

2.4 RT-qRCR

Mouse skin tissues were homogenized in TRIzol (Takara Bio Inc., Kusatsu, Shiga, Japan) using a Bead beater (Biospec), whereas cells were directly resuspended in TRIzol (Takara Bio Inc., Kusatsu, Shiga, Japan). Total RNAs were isolated and reverse transcribed into complementary DNA using the Revert Aid First Strand cDNA Synthesis Kit (Roche, F. Hoffmann-La Roche AG, Basel-Stadt, Switzerland) according to the manufacturer's instructions. The primers were synthetized as in Table 1 (Sangon Biotech Co., Ltd., Shanghai, China). RT–qPCR was performed in triplicate using SYBR green master mix (Roche, F. Hoffmann-La Roche AG, Basel-Stadt, Switzerland) on a Step One Plus Real-Time PCR System (Applied Biosystem, Thermo Fisher Scientific, Waltham, MA, USA). Samples with a low yield of RNA were predetermined and excluded. Results were normalized to glyceraldehyde-3-phosphate dehydrogenase (*GAPDH*) and the comparative $\Delta\Delta$CT method was used to determine the quantification of gene expression. The information of primers in Table 1.

2.5 RNA Sequencing Methodology

Total RNA was extracted from mice at 2rd day post-wound, and ribosomal RNA (rRNA), constituting >90% of total RNA, was depleted using a standard kit to enrich messenger RNA (mRNA). Eukaryotic mRNA was further enriched via Oligo (dT) magnetic bead selection for polyadenylated transcripts. This polyA-selected mRNA was fragmented ultrasonically. First-strand cDNA synthesis used fragmented mRNA, random hexamer primers, and M-MuLV Reverse Transcriptase. Following RNA template degradation (RNase H), second-strand cDNA synthesis was performed with DNA Polymerase I and dNTPs. Purified double-stranded cDNA (dscDNA) underwent end repair, 3′ adenylation (A-tailing), and ligation of standard Illumina sequencing adapters. cDNA fragments of ~200 bp were size-selected using AMPure XP beads (Beckman Coulter Life Sciences, Indianapolis, IN, USA), PCR amplified, and purified again with AMPure XP beads to generate the final library.

Table 1. Primers for RT–qPCR.

Primers	Sequence(5′ to 3′)	Melting Temperature (TM)	Length
IL-6-human-F	GGTACATCCTCGACGGCATCT	59.4	21
IL-6-human-R	GTGCCTCTTTGCTGCTTTCAC	57.5	21
IL-8-human-R	TCTCTTGGCAGCCTTCCT	56.2	18
IL-8-human-R	ACTGAACCTGACCGTACATGTCTTTATGCACTGACATCT	65.0	39
IL-1B-human-F	TACGAATCTCCGACCACCACTACAG	60.1	25
IL-1B-human-R	TGGAGGTGGAGAGCTTTCAGTTCATATG	60.0	28
ACTA2-human-F	ACTGAGCGTGGCTATTCCTCCGTT	62.9	24
ACTA2-human-R	GCAGTGGCCATCTCATTTTCA	55.8	21
GAPDH-human-F	CTGAGTACGTCGTGGAGTC	55.0	19
GAPDH-human-R	ACTGAACCTGACCGTACACAGAGATGATGACCCTTTG	65.9	38

Stringent quality control was applied: RNA integrity and DNA contamination were assessed by agarose gel electrophoresis; RNA purity (OD260/280, OD260/230) was measured using a NanoPhotometer spectrophotometer (Implen GmbH, Munich, Germany); RNA concentration was precisely quantified using a Qubit 2.0 Fluorometer (Thermo Fisher Scientific, Waltham, MA, USA); and RNA integrity was accurately determined using an Agilent 2100 Bioanalyzer (Agilent Technologies, Santa Clara, CA, USA).

Libraries were sequenced on the Illumina NovaSeq platform (Illumina, Inc., San Diego, CA, USA) using high-density flow cells. This system delivers high throughput (yielding up to 6 Tb and 20 billion reads per run), enabling sensitive detection of coding and diverse non-coding RNAs, even in challenging samples. The platform facilitates multiplexed sequencing of up to 400 transcriptomes per run.

2.6 In Vitro Studies

2.6.1 Cell Lines

The BJ (Cat no. GNHu49) and HaCat (Cat no. SCSP-5091) cells were kindly provided by Cell Bank, Chinese Academy of Sciences (National Collection of Authenticated Cell Cultures, Shanghai, China). BJ cells were treated with TGF-β1 (10 ng/mL, cat no. Ag24881, Proteintech Group, Inc, Rosemont, IL, USA) with/without quercetin (5–50 µM) for 72 h. All cell lines were validated by short tandem repeat (STR) profiling and tested negative for mycoplasma. Differentiation was assessed by alpha-smooth muscle actin (α-SMA) and collagen I and collagen III (qRT-PCR and western blot).

2.6.2 CCK-8 Analysis

The BJ or HaCat cells were seeded in a 96-well plate and treated with quercetin at different concentration for 24 h. The CCK-8 reagent was added to each well and incubated according to manufacturer instructions (cat no. C0037, Beyotime Biotechnology Co., Ltd. Shanghai, China), and the absorbance at 450 nm was measured to quantify cell viability.

2.6.3 Scratch Wound Assay

Confluent BJ fibroblasts and HacCaT were scratched separately with a 200 µL pipette tip, washed, and treated with quercetin (0–200 µM) or vehicle. Migration was imaged at 0, 6, 12, 24 and 48 h (phase-contrast microscope). Gap closure was quantified using Image J.

2.7 Statistical Analysis

Data are presented as Mean $\pm$ SD. One-way ANOVA with Tukey's post-hoc test was used for comparisons among three groups or more. For repeated measurement data or two-factor factorial design, Two-way ANOVA or Dunnett's multiple comparison test was used (GraphPad Prism, version 10, GraphPad Software, Inc., San Diego, CA, USA). Significance was set at $p < 0.05$.

3. Results

3.1 Quercetin Accelerates Early Wound Closure in BALB/c Mice

Topical application of 1% quercetin significantly enhanced wound healing in the murine excisional model, and topical application of 1% TGF-β was used as a positive control, because the factor would regulate multiple phases including inflammation, proliferation, and remodeling during wound healing and stimulate excessive collagen deposition and myofibroblast differentiation during scar formation [29,30]. By day 6, quercetin-treated wounds achieved significantly smaller area, showing as 0.028 ± 0.003 cm^2 closure compared with 0.041 ± 0.002 cm^2 in the vehicle control group and 0.034 ± 0.001 cm^2 in the TGF-β group (Fig. 1A,B, $p < 0.05$). Histological analysis (H&E staining) confirmed reduced inflammatory cell infiltration and accelerated granulation tissue formation in quercetin-treated wounds compared with the other two groups (Fig. 1C), and the epidermis thickness of quercetin treatment was significantly smaller than the control group based on H&E staining (Fig. 1E, $p < 0.05$). In addition, Ki-67 immunohistochemistry showed an increase in proliferating cells within the quercetin-treated wound bed on day 6, localized predominantly to the epidermal margins and dermal papillae (Fig. 1D,F, $p < 0.05$).

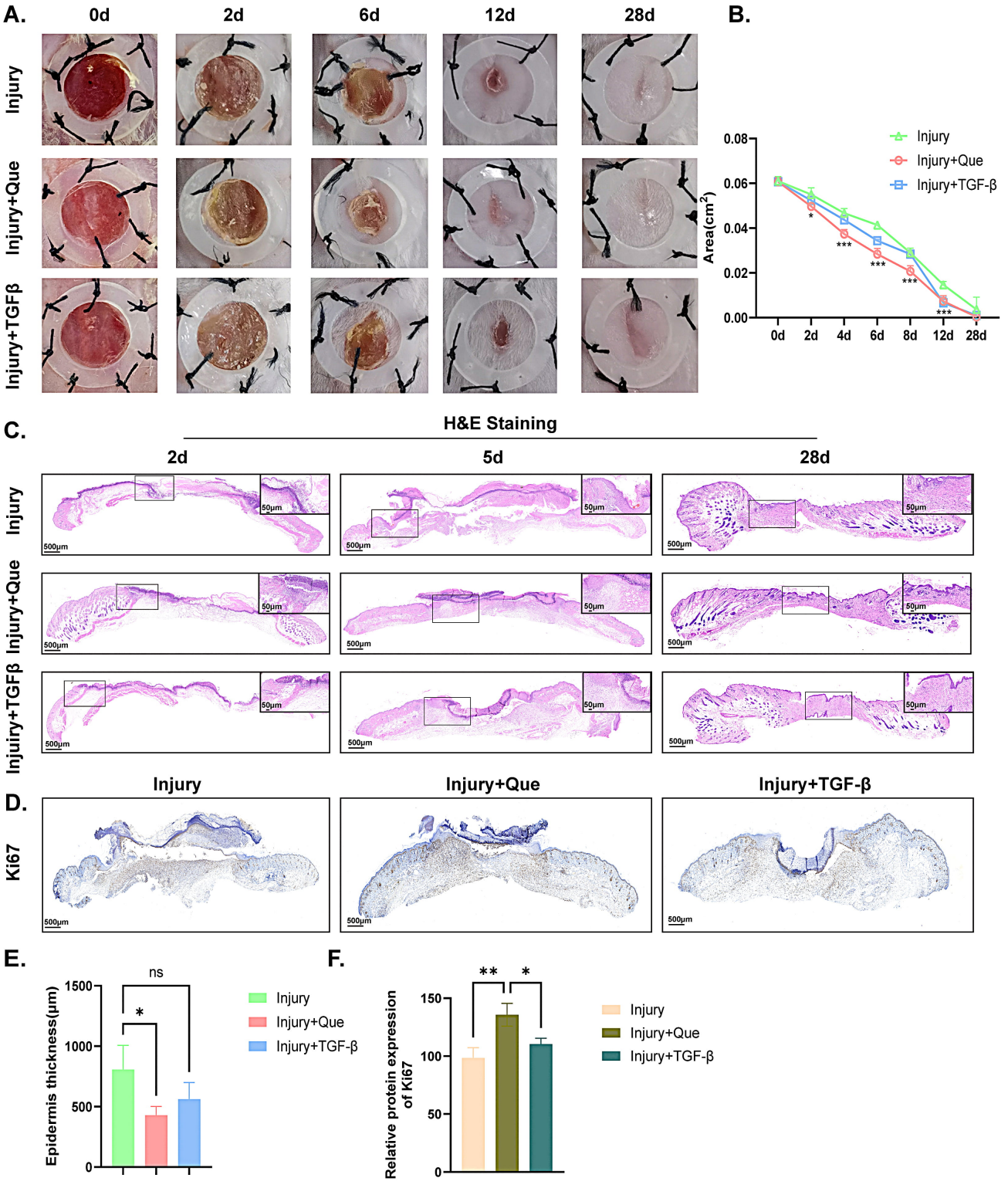

Fig. 1. Quercetin accelerates early wound closure in Mice. (A,B) Photographs of the gross appearance of wound healing in mice and the statistical analysis. (C) HE staining of wound on the 2nd, 5th and 28th day among the three groups. (D) IHC staining of Ki-67 on the 6th day among the three groups. (E) Statistical analysis of epidermis thickness of wound in mice according to HE staining. (F) Quantitative analysis of Ki-67 expression in wound among the three groups. Scale bar = 500 μm or 50 μm. * $p < 0.05$, ** $p < 0.01$, *** $p < 0.001$, and ns, not significant when compared between each group. n = 3~5 in each animal group. The data are shown as the mean ± SD. One-way ANOVA for (E,F) and Two-way ANOVA for (B) were used for multiple group comparisons. IHC, Immunohistochemistry.

3.2 Regulation of Inflammatory Response With Quercetin

To further elucidate potential targets and signaling pathways involved in quercetin-mediated wound healing, wound tissue was harvested from the vehicle control group and 1% quercetin treated group on the 2nd day, and analyzed with RNA sequencing (RNA-seq). According to previous study, day 2 (approximately 48 hours) post-wounding is a well-suited time point for analyzing the inflammatory response during wound healing, as it captures peak neutrophil and early macrophage activity, along with cytokine and growth factor expression [31]. Considering that the strong anti-inflammatory capability of quercetin, we hypothesized that the promotion of skin healing by quercetin may be related to its anti-inflammatory properties. As shown in Fig. 2A, a total of 21,991 differentially expressed genes were screened out, of which 1157 genes were upregulated and 1254 genes were downregulated, as evidenced by the volcano plot. Furthermore, the enrichment analysis results from Go term, KEGG pathways and Reactome pathways indicated that the differentially expressed genes primarily affected the inflammatory response, such as NLRP3 inflammasome complex, inflammasome-mediated signaling pathway and so on (Fig. 2B–D). Heating map and chord diagram suggested that the inflammation-related genes of *NLRP1B, DDX3X, LFI213, IRGM2* and *PYCARD* were significantly down-regulated in quercetin treated group when compared with the vehicle control group, as depicted in Fig. 2E,F. Taken together, the application of quercetin may regulate the inflammatory response during wound healing.

3.3 Suppression of Pro-Inflammatory Cytokines

Based on the transcriptomic data, we further validated that quercetin treatment markedly attenuated inflammation during the early phase of wound repair. The results of immunofluorescence in mice revealed significant reduction in IL-1β and caspase-1 in wound lysates on day 2 when compared with the vehicle control group and the TGF-β treatment group, as depicted in Fig. 3A,B ($p < 0.05$). To further explore the anti-inflammatory effect, BJ and HaCat cell was used for *in vitro* study. HaCaT acting as keratinocytes model the epidermal layer, while BJ acting as fibroblasts represented the dermal layer, reflecting their respective roles in skin structure and wound healing. They were treated with varying doses of quercetin and the CCK-8 result suggested the drug was safe at the concentration ranging from 10 µM to 200 µM for HaCat cell, while the safe dosage was 50 µM for BJ cell, as shown in Fig. 3C ($p < 0.05$). In BJ cells, with the safe dose of quercetin at 50 µM, the protein expression of ACS ($p < 0.05$), Caspase-1 ($p < 0.05$), and IL-1β ($p < 0.05$) were significantly lower than the NC group (Fig. 3D,E). In HaCat cells, within the safe dose ranging from 10 µM to 200 µM, the protein expression of ACS was only lower than the NC group at 200 µM ($p < 0.05$), while Caspase-1 was lower than the NC group at 10 µM ($p < 0.05$), 50 µM ($p < 0.05$), 100 µM ($p < 0.05$), and 200 µM ($p < 0.05$). IL-1β was lower than the NC group at 10–200 µM (Fig. 3F,G, $p < 0.05$). Therefore, except for ACS in HaCat cells, quercetin at 50 µM significantly inhibited the expression of inflammatory proteins in both BJ and HaCat cells, although a dose-response trend was observed across all tested concentrations. In addition, the results of qRT-PCR are different with the results of western-blot analysis in Fig. 3H,I. Under high concentration stimulation of quercetin, the inhibition of IL-1β protein levels in keratinocytes is mainly due to its inhibition of inflammatory signaling pathways (NF-κB, NLRP3) and receptors (such as IL1R1), blocking protein maturation and secretion. And gene expression may increase due to imbalanced transcription factor networks (such as YY1 inhibition release), epigenetic modifications, or negative feedback regulation. At the same time, keratinocytes have specific regulatory mechanisms, and certain stimuli can induce *IL-1B* gene transcription without protein secretion. Quercetin may amplify this transcription translation decoupling effect. Therefore, quercetin can effectively inhibit the inflammatory response during the skin healing process *in vivo* and *in vitro*.

3.4 Modulation of Collagen Deposition and Scar Quality

According to the wound healing image on day 28 (Fig. 4A), the positive drug TGF- β1 can indeed promote early wound healing. However, we found that on day 28, the pigmentation and scar formation at the wound site were significantly greater than those in the quercetin group, moreover even exceeded the control group. The scars in the quercetin group were the lightest, so our future research will investigate whether quercetin inhibits scar formation during tissue remodeling. First, we measured the scar size of the control group, quercetin group, and TGF-β1 group on day 28. We found that the scar length was reduced in the quercetin group (Fig. 4B, $p < 0.05$). In addition, Masson's trichrome staining demonstrated that quercetin improved collagen architecture during the remodeling phase (day 28, Fig. 4C). The collagen III/I ratio in quercetin-treated scars was significantly higher than in the control group (Fig. 4D,F, $p < 0.05$). Additionally, α-SMA, as a marker of myofibroblasts and scars, showed significantly lower expression in the quercetin-treated group than the control group, which detected by immunofluorescence in the dermis (Fig. 4E,G, $p < 0.05$).

3.5 Inhibition of TGF-β1-Induced Myofibroblast Differentiation

To further investigate the differentiation effect of quercetin on fibroblasts into myofibroblasts, the BJ cells were treated with quercetin only and quercetin with TGF-β1. As depicted in Fig. 5A–C, low concentration of quercetin (20–50 µM) effectively suppressed TGF-β1-driven myofibroblast differentiation, showing as decrease in α-SMA expression of genes and protein, while the high concentration (100 µM) showed the opposite effect as pro-

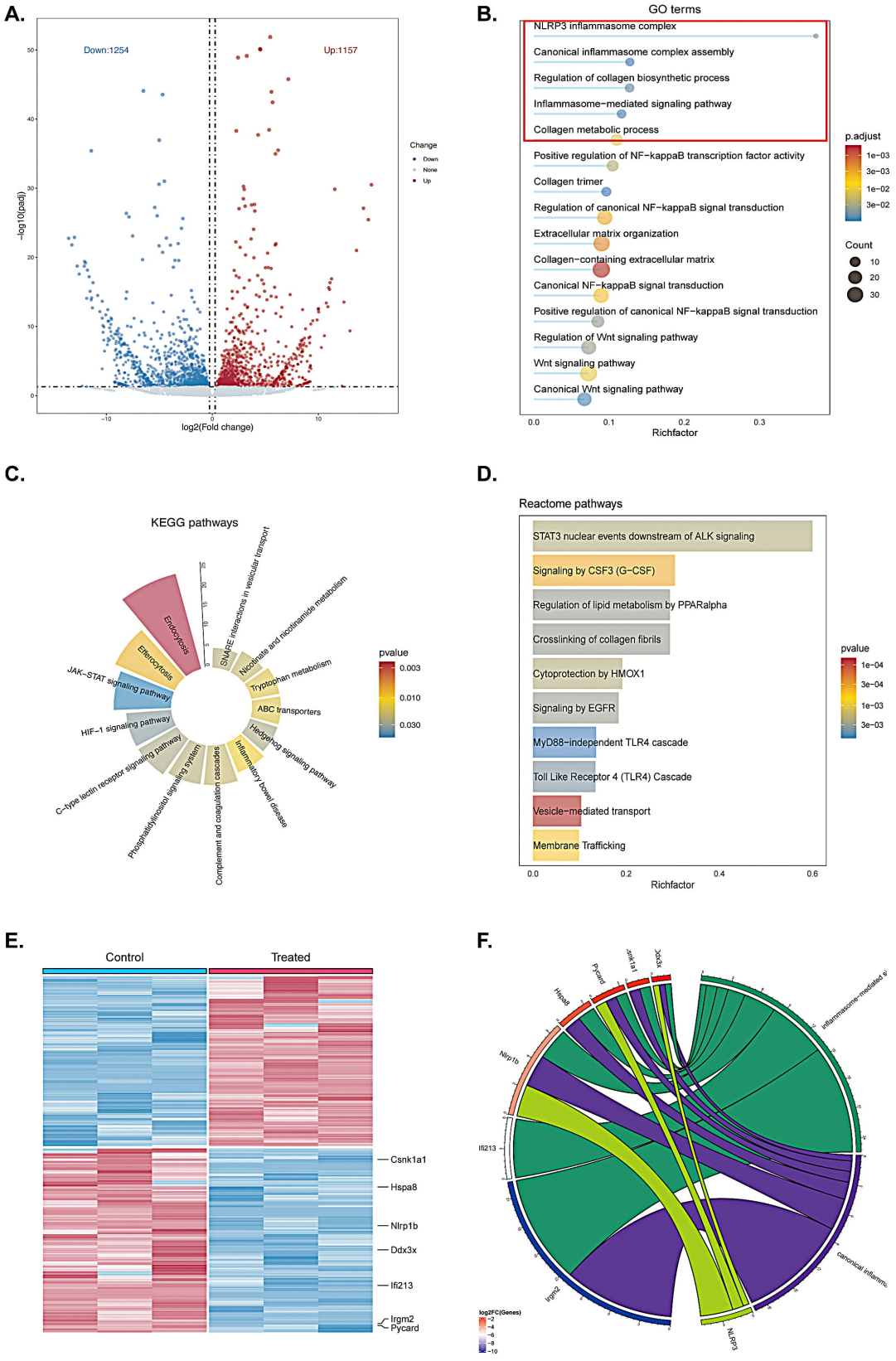

Fig. 2. Quercetin regulates the inflammatory response during early wound closure in mice. (A) Volcano plot illustrating the differentially expressed genes between the vehicle control group and the quercetin treated group. (B–D) Enrichment analyses of GO term, KEGG pathways, and Reactome pathways comparing the two groups. Inflammatory response related pathways are highlighted with red boxes in the GO terms. (E,F) Heat map and chord diagram depicting the inner relationships among differentially expressed genes. n = 3 in each animal group.

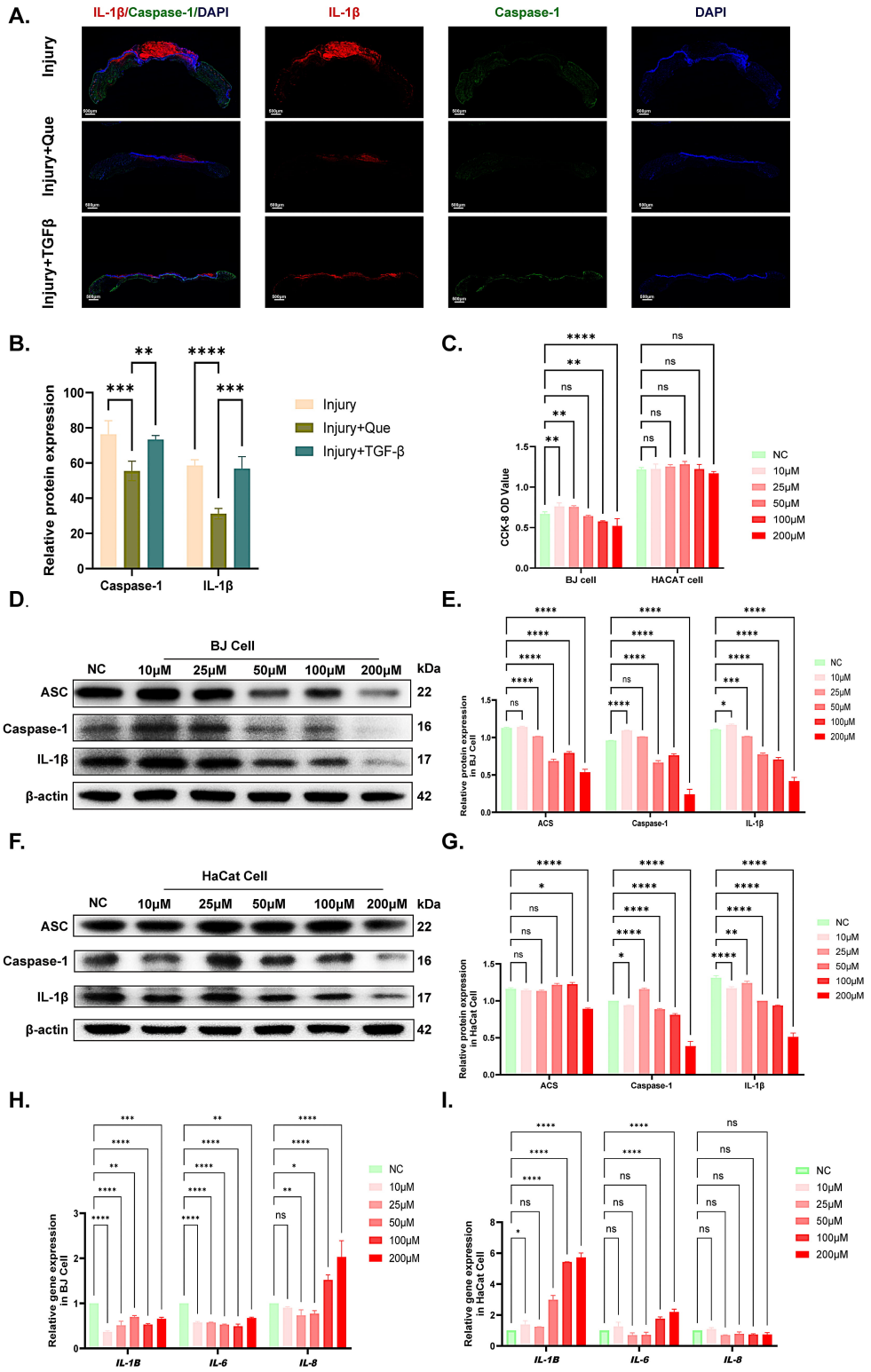

Fig. 3. Suppression of pro-inflammatory cytokines in quercetin-treated wound healing. (A,B) IF staining and quantitative analyses of CASPASE-1 and IL-1β on the 2nd day of wound healing among the three. (C) BJ and HaCat cell vitality analyses when treated with quercetin at gradient increasing concentration. (D–G) Western-blot analysis of ACS, CASPASE-1, IL-1β in BJ and HaCat cells when treated with quercetin in a dose-response manner (normalized to internal β-actin). (H,I) Analysis of gene expression of pro-inflammatory cytokines: IL-1β, IL-6 and IL-8 in BJ and HaCat cells treated with quercetin. Scale bar = 500 μm. * $p < 0.05$, ** $p < 0.01$, *** $p < 0.001$, **** $p < 0.0001$, and ns, not significant when compared between each group. The data are shown as the mean ± SD. n = 3~5 for each animal group. Two-way ANOVA with Dunnett multiple comparison test were used for multiple group comparisons. IL, Interleukin; IF, Immunofluorescence; NC, negative control; DAPI, 4′,6-diamidino-2-phenylindole.

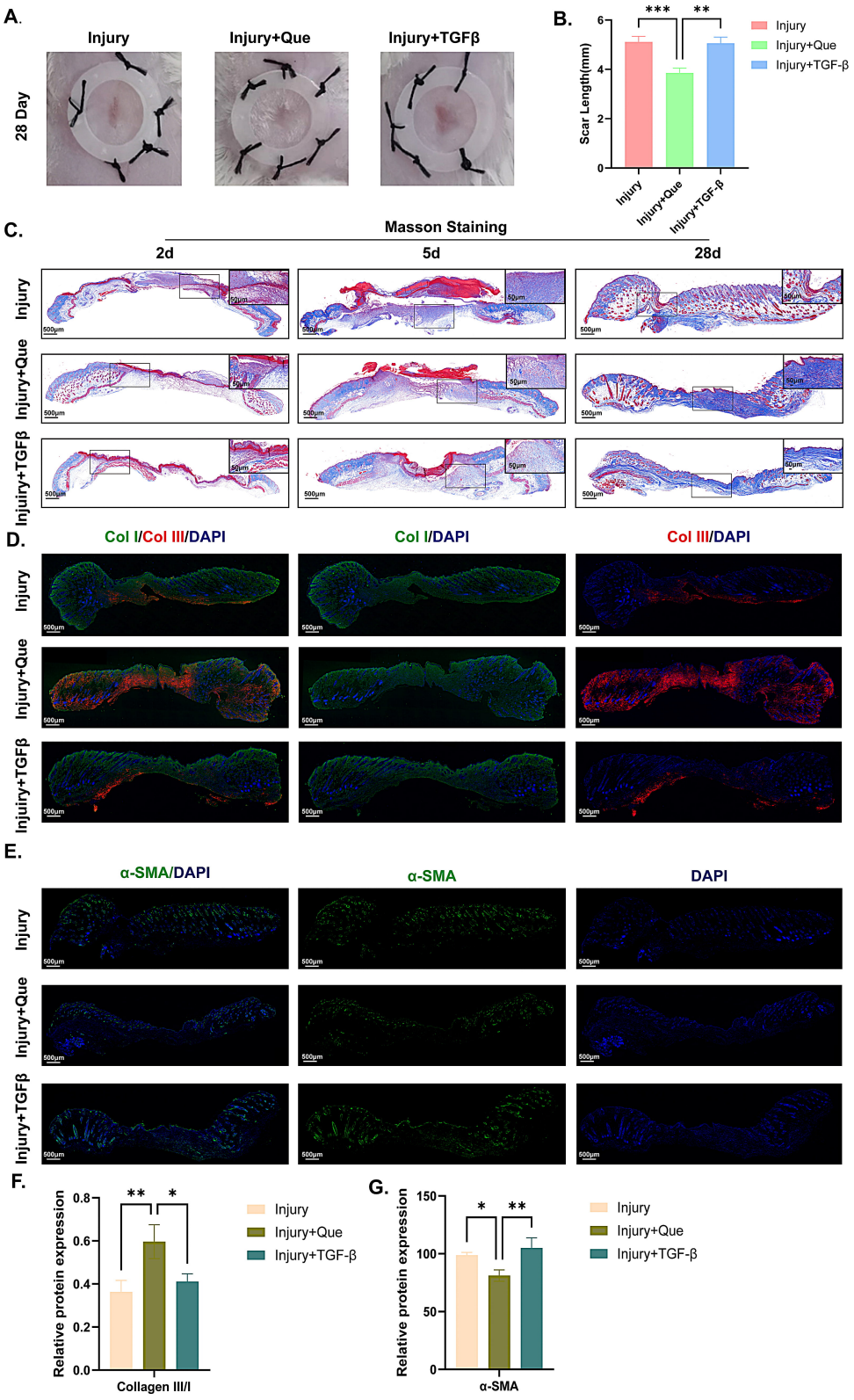

Fig. 4. Quercetin modulated collagen deposition and improved scar quality. (A,B) Photographs of scar length and statistical analysis among three groups. (C) Masson staining of wound quality on the 28th day among three groups. (D,E) IF staining of Collagen I/III and α-SMA in wound on the 28th day among three groups. (F,G) Statistical analysis of Ki-67 and ration between Collagen III/I among three groups. Scale bar = 500 μm or 50 μm. * $p < 0.05$, ** $p < 0.01$, and *** $p < 0.001$ when compared between each group. The data are shown as the mean ± SD. n = 3~5 for each group. Two-way ANOVA for (B,F,G) were used for multiple group comparisons. α-SMA, alpha-smooth muscle actin.

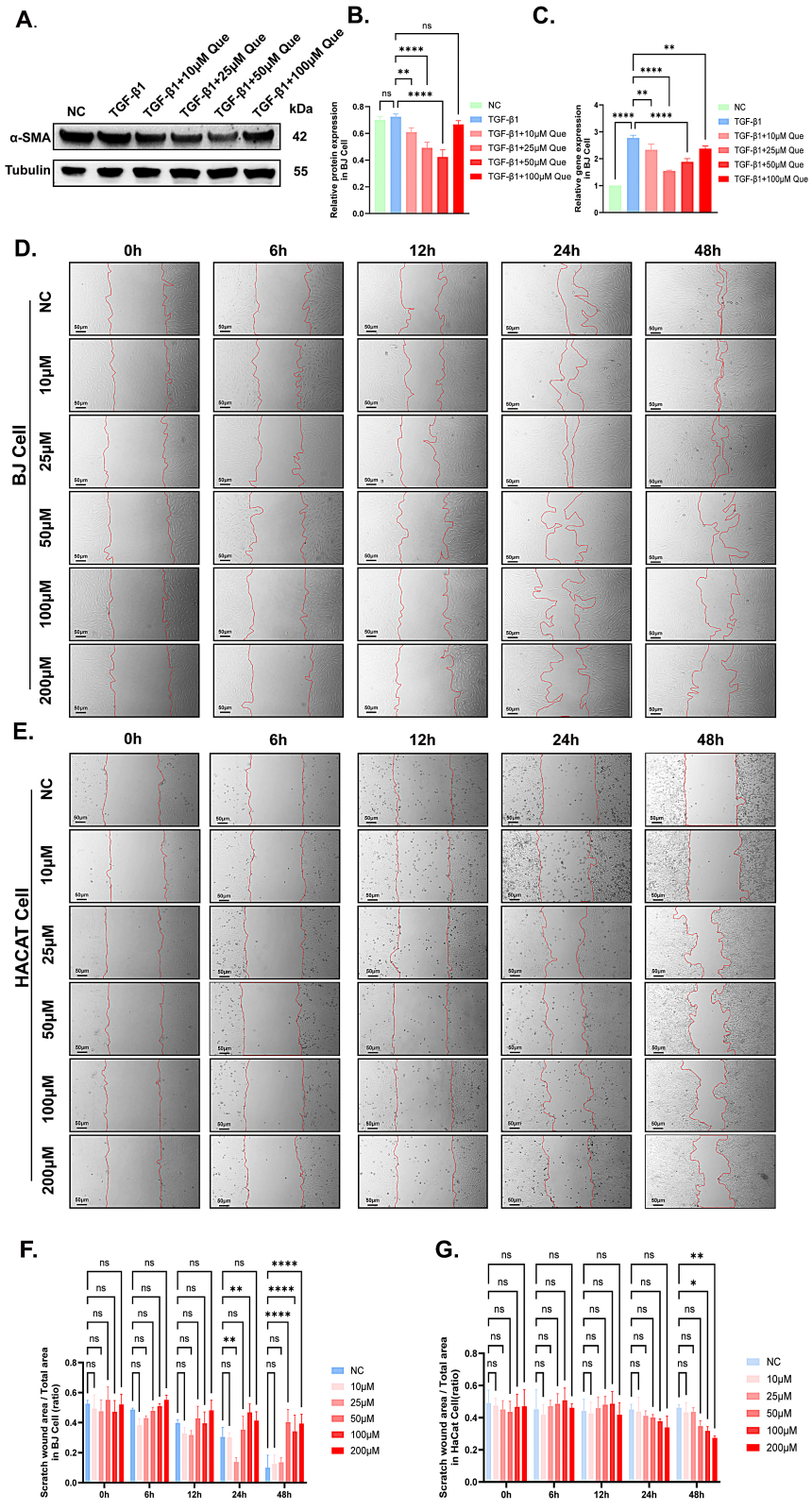

Fig. 5. Quercetin inhibited TGF-β1-Induced myofibroblast differentiation. (A,B) Western-blot analysis of α-SMA expression when TGF-β1-induced BJ cells are treated with quercetin. (C) Gene expression of *ACTA2* in TGF-β1-induced BJ cells treated with quercetin. (D,E) Scratch wound assay of BJ and HaCat cells treated with quercetin in a dose-response manner. (F,G) Statistical analysis of the scratch wound assay of BJ and HaCat cells. Scale bar = 50 μm. * $p < 0.05$, ** $p < 0.01$, and **** $p < 0.0001$, and ns, not significant when compared between each group. The data are shown as the mean ± SD. One-way ANOVA for (B,C) or Two-way ANOVA for (F,G) was used for multiple group comparisons. TGF-β, transforming growth factor beta.

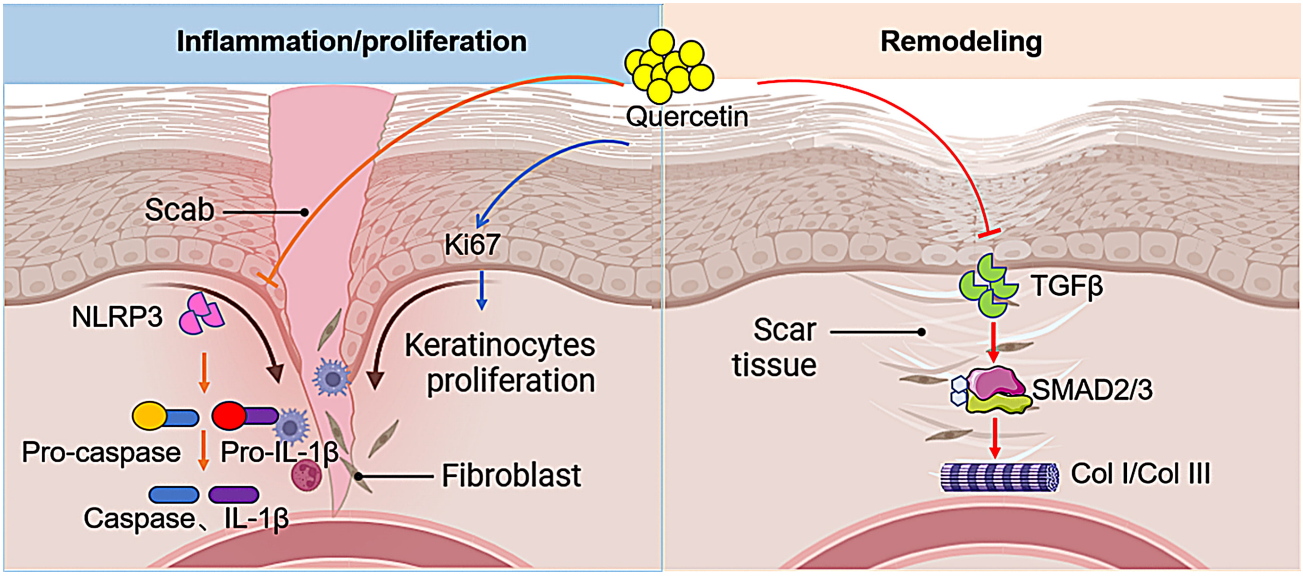

Fig. 6. Schematic diagram of quercetin in promoting early wound healing and attenuating scar formation (created by BioRender.com).

moting myofibroblast differentiation ($p < 0.05$). Since HaCaT cells acting as keratinocytes model the epidermal layer, while BJ acting as fibroblasts represented the dermal layer, reflecting their respective roles in skin structure and wound healing. During skin wound healing and scar formation, increased migration of HaCaT cells reflects enhanced epidermal re-epithelialization, while elevated collagen production by BJ fibroblasts indicates dermal matrix remodeling, consistent with their roles in skin repair. A similar trend was found in the scratch wound assay that, in BJ and HaCat cells, quercetin attenuated BJ fibroblast migration, and increased the proliferation of HaCat cells, with the statistical difference, as shown in Fig. 5D–G ($p < 0.05$). These results are consistent with Fig. 1, where quercetin promotes Ki-67 expression in the early stages of wound healing. On the one hand, it promotes wound healing by inducing proliferation, and on the other hand, it alleviates scar formation by inhibiting BJ fibroblast differentiation into myofibroblasts.

4. Discussion

Quercetin's early anti-inflammatory, which involves inhibiting NF-κB-mediated cytokine production, aligns perfectly with its role in facilitating the crucial transition to the proliferative phase of wound healing [32]. The observed shift in the collagen III/I ratio suggests a preferential synthesis of flexible fibrils, critical for pliable scarless healing. Furthermore, quercetin's ability to suppress myofibroblast differentiation via SMAD7 induction and SMAD2/3 blockade reveals a strategic dual-node intervention in TGF-β signaling This mechanism is notably distinct from that of direct receptor kinase inhibitors [33]. The dual role of quercetin in accelerating early wound healing while mitigating scar formation represents a significant advancement in the development of multifunctional wound therapeutics. Our findings demonstrate that quercetin orchestrates a balanced interplay between pro-healing and anti-fibrotic mechanisms, addressing two critical challenges in wound repair: delayed closure and pathological scarring (Fig. 6). Below, we contextualize these results within the broader scientific landscape and propose further mechanistic insights.

The accelerated wound closure observed in quercetin-treated mice aligns with its potent anti-inflammatory properties. By suppressing IL-1β and caspase-1 (key mediators of the NLRP3 inflammasome pathway), quercetin likely reduces pyroptosis and neutrophil-driven tissue damage during the inflammatory phase. This is consistent with prior studies showing that NLRP3 inhibition can accelerate diabetic wound healing by dampening excessive inflammation [34]. Concurrently, the upregulation of IL-10—a cytokine critical for macrophage polarization toward an M2 pro-resolving phenotype—suggests that quercetin fosters a regenerative microenvironment [35]. The observed 35% increase in Ki-67+ proliferating cells further underscores its role in promoting re-epithelialization, likely via enhanced keratinocyte and dermal papilla cell activity. These dual actions (anti-inflammatory + pro-proliferative) mirror the effects of other bioactive flavonoids, such as apigenin, which similarly enhance healing through cytokine modulation [36,37].

The marked increase in the collagen III/I ratio (1.8 vs. 0.9 in controls) in quercetin-treated scars vividly highlights its ability to guide steer collagen synthesis toward a more regenerative phenotype. Type III collagen, characterized by its finer fibrillar structure, is a hallmark of fetal wound healing—a process known for scarless repair [38,39]. In stark contrast, excessive type I collagen deposition, as seen observed in the TGF-β1-treated group, directly correlates

with rigid scar formation and poor functional outcomes. Notably, the elevated scar pigmentation and collagen density in the TGF-β1 group despite accelerated initial healing, reinforces the notion that unchecked TGF-β signaling exacerbates fibrosis, even if early closure is achieved. Quercetin's ability to suppress α-SMA expression and myofibroblast differentiation further disrupts the fibrotic cascade, as myofibroblasts are the primary drivers of collagen contraction and scar maturation [40,41].

The seemingly paradoxical observation that quercetin inhibits BJ fibroblast migration (scratch assay) while simultaneously promoting keratinocyte proliferation (Ki-67+ cells) underscores its cell type-specific activity. The suppression of fibroblast migration may prevent excessive myofibroblast recruitment and ECM contraction. Meanwhile, enhanced keratinocyte activity ensures rapid epithelial coverage—a balance critical for scarless healing. Similar cell-selective effects have been reported for compounds like asiaticoside, which promotes keratinocyte migration but inhibits fibroblast proliferation [42]. This inherent duality positions quercetin as a tunable agent capable of addressing distinct phases of repair.

Although our study provides robust preclinical evidence, several limitations warrant consideration. In terms of bioavailability, the efficacy of topical quercetin may be constrained by its poor skin penetration. Further research should explore nanocarriers, like lipid-based nanoparticles, to enhance delivery, similar to strategies used for curcumin in burn wounds [43].

In terms of outcomes, our scar quality assessments were limited to day 28; extended studies are needed to evaluate late remodeling (including assessments of tensile strength at 6 months). Mechanistically, future investigations could involve performing RNA sequencing on skin tissue samples from both quercetin treated and control groups on the 28th day to screen for key factors regulating fibroblast differentiation via the TGF-β signaling pathway. In addition, exploring synergistic combinations and epigenetic modulation, such as investigating quercetin's impact on TGF-β-associated miRNAs, could uncover additional anti-fibrotic mechanisms in future research.

5.Conclusion

Quercetin emerges as a bifunctional agent that harmonizes inflammation resolution, epithelial proliferation, and anti-fibrotic signaling to achieve scar-minimized wound repair. By temporally modulating TGF-β signaling, it addresses the dual challenges of delayed closure and fibrosis, offering a holistic approach to regenerative medicine. In clinical, these findings suggest that quercetin may serve as a promising regenerative agent to promote wound healing of skin and reduce scar formation. Future studies should explore combinatorial strategies with bioactive dressings to optimize delivery and efficacy.

Abbreviations

TGF-β, Transforming Growth Factor beta; IL-1β, Interleukin-1 Beta; α-SMA, Alpha-Smooth Muscle Actin; H&E, Hematoxylin and Eosin; i.p., intraperitoneal injection; IHC, Immunohistochemistry; IF, Immunofluorescence.

Availability of Data and Materials

All data supporting the findings of the present study are available within the paper or from the corresponding author upon reasonable request.

Author Contributions

The study was designed by DW, MYJ and JZ were involved in its execution. DW and MYJ handled data collection and analysis. DW and JZ contributed to drafting the manuscript. All authors contributed to editorial changes in the manuscript. All authors read and approved the final manuscript. All authors have participated sufficiently in the work and agreed to be accountable for all aspects of the work.

Ethics Approval and Consent to Participate

This research was approved by the Animal Ethics Committee of the Eye & ENT Hospital of Fudan University (Ethical approval numbers: 2020096). The care and protection of experimental animals were in accordance with the protocols of the National Institutes of Health Guide for the Care and Use of Laboratory Animals (NIH Publications No. 8023, revised 1978).

Acknowledgment

We thank LetPub for its linguistic assistance during the preparation of this manuscript.

Funding

This study was supported by grants from the National Natural Science Foundation of China (82171020, 81900817).

Conflict of Interest

The authors declare no conflict of interest.

References

[1] Guo S, Dipietro LA. Factors affecting wound healing. Journal of Dental Research. 2010; 89: 219–229. https://doi.org/10.1177/0022034509359125.

[2] Li Z, Ma R, Tan J, Li C, Xiao Y, Qiu X, *et al*. Hormonal interventions in skin wounds - a mini review. Molecular Medicine (Cambridge, Mass.). 2024; 30: 217. https://doi.org/10.1186/s10020-024-00978-6.

[3] Conforti P, Martínez Santamaría JC, Schachtrup C. Fibrinogen: connecting the blood circulatory system with CNS scar formation. Frontiers in Cellular Neuroscience. 2024; 18: 1402479. https://doi.org/10.3389/fncel.2024.1402479.

[4] Cioce A, Cavani A, Cattani C, Scopelliti F. Role of the Skin Immune System in Wound Healing. Cells. 2024; 13: 624. https://doi.org/10.3390/cells13070624.
[5] Li S, Yang P, Ding X, Zhang H, Ding Y, Tan Q. Puerarin improves diabetic wound healing via regulation of macrophage M2 polarization phenotype. Burns & Trauma. 2022; 10: tkac046. https://doi.org/10.1093/burnst/tkac046.
[6] Li X, Zhang D, Yu Y, Wang L, Zhao M. Umbilical cord-derived mesenchymal stem cell secretome promotes skin regeneration and rejuvenation: From mechanism to therapeutics. Cell Proliferation. 2024; 57: e13586. https://doi.org/10.1111/cpr.13586.
[7] Tucci M, Hildebrandt D, Lichtenhan J, Benghuzzi H. Evaluation of Full Thickness Wounds Following Application of a Visco-Liquid Hemostat in a Swine Model. Pathophysiology: the Official Journal of the International Society for Pathophysiology. 2024; 31: 458–470. https://doi.org/10.3390/pathophysiology31030034.
[8] Chandra P, Faizan M, Porwal M, Sharma H, Sachan N. An Overview and Review of Growth Factors in Wound Healing: Emerging Trends and Innovations. Current Diabetes Reviews. 2025. https://doi.org/10.2174/0115733998332692241202072249. (online ahead of print)
[9] Peña OA, Martin P. Cellular and molecular mechanisms of skin wound healing. Nature Reviews. Molecular Cell Biology. 2024; 25: 599–616. https://doi.org/10.1038/s41580-024-00715-1.
[10] Tan ZX, Tao R, Li SC, Shen BZ, Meng LX, Zhu ZY. Role of defensins in diabetic wound healing. World Journal of Diabetes. 2022; 13: 962–971. https://doi.org/10.4239/wjd.v13.i11.962.
[11] Liu M, López de Juan Abad B, Cheng K. Cardiac fibrosis: Myofibroblast-mediated pathological regulation and drug delivery strategies. Advanced Drug Delivery Reviews. 2021; 173: 504–519. https://doi.org/10.1016/j.addr.2021.03.021.
[12] Wang AS, Armstrong EJ, Armstrong AW. Corticosteroids and wound healing: clinical considerations in the perioperative period. American Journal of Surgery. 2013; 206: 410–417. https://doi.org/10.1016/j.amjsurg.2012.11.018.
[13] Lee JH, Massagué J. TGF-β in developmental and fibrogenic EMTs. Seminars in Cancer Biology. 2022; 86: 136–145. https://doi.org/10.1016/j.semcancer.2022.09.004.
[14] Ong CH, Tham CL, Harith HH, Firdaus N, Israf DA. TGF-β-induced fibrosis: A review on the underlying mechanism and potential therapeutic strategies. European Journal of Pharmacology. 2021; 911: 174510. https://doi.org/10.1016/j.ejphar.2021.174510.
[15] Rafiq RA, Quadri A, Nazir LA, Peerzada K, Ganai BA, Tasduq SA. A Potent Inhibitor of Phosphoinositide 3-Kinase (PI3K) and Mitogen Activated Protein (MAP) Kinase Signalling, Quercetin (3, 3', 4', 5, 7-Pentahydroxyflavone) Promotes Cell Death in Ultraviolet (UV)-B-Irradiated B16F10 Melanoma Cells. PloS One. 2015; 10: e0131253. https://doi.org/10.1371/journal.pone.0131253.
[16] González-Restrepo D, Zuluaga-Vélez A, Orozco LM, Sepúlveda-Arias JC. Silk fibroin-based dressings with antibacterial and anti-inflammatory properties. European Journal of Pharmaceutical Sciences: Official Journal of the European Federation for Pharmaceutical Sciences. 2024; 195: 106710. https://doi.org/10.1016/j.ejps.2024.106710.
[17] Zhou Y, Qian C, Tang Y, Song M, Zhang T, Dong G, *et al*. Advance in the pharmacological effects of quercetin in modulating oxidative stress and inflammation related disorders. Phytotherapy Research: PTR. 2023; 37: 4999–5016. https://doi.org/10.1002/ptr.7966.
[18] Ismail EN, Zakuan N, Othman Z, Vidyadaran S, Mohammad H, Ishak R. Polyphenols mitigating inflammatory mechanisms in inflammatory bowel disease (IBD): focus on the NF-κB and JAK/STAT pathways. Inflammopharmacology. 2025; 33: 759–765. https://doi.org/10.1007/s10787-024-01607-8.
[19] Xu D, Hu MJ, Wang YQ, Cui YL. Antioxidant Activities of Quercetin and Its Complexes for Medicinal Application. Molecules (Basel, Switzerland). 2019; 24: 1123. https://doi.org/10.3390/molecules24061123.
[20] Sahoo DK, Heilmann RM, Paital B, Patel A, Yadav VK, Wong D, *et al*. Oxidative stress, hormones, and effects of natural antioxidants on intestinal inflammation in inflammatory bowel disease. Frontiers in Endocrinology. 2023; 14: 1217165. https://doi.org/10.3389/fendo.2023.1217165.
[21] Peng D, Fu M, Wang M, Wei Y, Wei X. Targeting TGF-β signal transduction for fibrosis and cancer therapy. Molecular Cancer. 2022; 21: 104. https://doi.org/10.1186/s12943-022-01569-x.
[22] Budi EH, Schaub JR, Decaris M, Turner S, Derynck R. TGF-β as a driver of fibrosis: physiological roles and therapeutic opportunities. The Journal of Pathology. 2021; 254: 358–373. https://doi.org/10.1002/path.5680.
[23] Hu HH, Chen DQ, Wang YN, Feng YL, Cao G, Vaziri ND, *et al*. New insights into TGF-β/Smad signaling in tissue fibrosis. Chemico-biological Interactions. 2018; 292: 76–83. https://doi.org/10.1016/j.cbi.2018.07.008.
[24] Zhang X, Cai Y, Zhang W, Chen X. Quercetin ameliorates pulmonary fibrosis by inhibiting SphK1/S1P signaling. Biochemistry and Cell Biology. 2018; 96: 742–751. https://doi.org/10.1139/bcb-2017-0302.
[25] Geng F, Zhao L, Cai Y, Zhao Y, Jin F, Li Y, *et al*. Quercetin Alleviates Pulmonary Fibrosis in Silicotic Mice by Inhibiting Macrophage Transition and TGF-β-Smad2/3 Pathway. Current Issues in Molecular Biology. 2023; 45: 3087–3101. https://doi.org/10.3390/cimb45040202.
[26] Afarin R, Hatami M, Monjezi S, Bineshfar F, Ahangarpour A. Suppression of TGF-β/Smad3 signaling pathway by *Capparis spinosa* and quercetin in a rat model of nonalcoholic steatohepatitis. Iranian Journal of Basic Medical Sciences. 2024; 27: 1096–1104. https://doi.org/10.22038/IJBMS.2024.76264.16497.
[27] Marshall CD, Hu MS, Leavitt T, Barnes LA, Cheung ATM, Malhotra S, *et al*. Sanativo Wound Healing Product Does Not Accelerate Reepithelialization in a Mouse Cutaneous Wound Healing Model. Plastic and Reconstructive Surgery. 2017; 139: 343–352. https://doi.org/10.1097/PRS.0000000000003013.
[28] El Gazaerly H, Elbardisey DM, Eltokhy HM, Teaama D. Effect of transforming growth factor Beta 1 on wound healing in induced diabetic rats. International Journal of Health Sciences. 2013; 7: 160–172. https://doi.org/10.12816/0006040.
[29] Penn JW, Grobbelaar AO, Rolfe KJ. The role of the TGF-β family in wound healing, burns and scarring: a review. International Journal of Burns and Trauma. 2012; 2: 18–28.
[30] Finnson KW, McLean S, Di Guglielmo GM, Philip A. Dynamics of Transforming Growth Factor Beta Signaling in Wound Healing and Scarring. Advances in Wound Care. 2013; 2: 195–214. https://doi.org/10.1089/wound.2013.0429.
[31] Kim MH, Liu W, Borjesson DL, Curry FRE, Miller LS, Cheung AL, *et al*. Dynamics of neutrophil infiltration during cutaneous wound healing and infection using fluorescence imaging. The Journal of Investigative Dermatology. 2008; 128: 1812–1820. https://doi.org/10.1038/sj.jid.5701223.
[32] Aggarwal D, Chaudhary M, Mandotra SK, Tuli HS, Chauhan R, Joshi NC, *et al*. Anti-inflammatory potential of quercetin: From chemistry and mechanistic insight to nanoformulations. Current Research in Pharmacology and Drug Discovery. 2025; 8: 100217. https://doi.org/10.1016/j.crphar.2025.100217.
[33] Singh D, Rai V, Agrawal DK. Regulation of Collagen I and Collagen III in Tissue Injury and Regeneration. Cardiology and Cardiovascular Medicine. 2023; 7: 5–16. https://doi.org/10.26502/fccm.92920302.

[34] Lv D, Cao X, Zhong L, Dong Y, Xu Z, Rong Y, *et al*. Targeting phenylpyruvate restrains excessive NLRP3 inflammasome activation and pathological inflammation in diabetic wound healing. Cell Reports. Medicine. 2023; 4: 101129. https://doi.org/10.1016/j.xcrm.2023.101129.

[35] Liu X, Tao T, Yao H, Zheng H, Wang F, Gao Y. Mechanism of action of quercetin in rheumatoid arthritis models: meta-analysis and systematic review of animal studies. Inflammopharmacology. 2023; 31: 1629–1645. https://doi.org/10.1007/s10787-023-01196-y.

[36] Ginwala R, Bhavsar R, Chigbu DI, Jain P, Khan ZK. Potential Role of Flavonoids in Treating Chronic Inflammatory Diseases with a Special Focus on the Anti-Inflammatory Activity of Apigenin. Antioxidants (Basel, Switzerland). 2019; 8: 35. https://doi.org/10.3390/antiox8020035.

[37] D'Amico E, Pierfelice TV, Iezzi G, Di Pietro N, Lepore S, Lorusso F, *et al*. Apigenin promotes proliferation and mineralization of human osteoblasts and up-regulates osteogenic markers. Applied Sciences. 2022; 12: 8510. https://doi.org/10.3390/app12178510.

[38] Gardeazabal L, Izeta A. Elastin and collagen fibres in cutaneous wound healing. Experimental Dermatology. 2024; 33: e15052. https://doi.org/10.1111/exd.15052.

[39] Leung A, Crombleholme TM, Keswani SG. Fetal wound healing: implications for minimal scar formation. Current Opinion in Pediatrics. 2012; 24: 371–378. https://doi.org/10.1097/MOP.0b013e3283535790.

[40] Schuster R, Younesi F, Ezzo M, Hinz B. The Role of Myofibroblasts in Physiological and Pathological Tissue Repair. Cold Spring Harbor Perspectives in Biology. 2023; 15: a041231. https://doi.org/10.1101/cshperspect.a041231.

[41] Hinz B. Myofibroblasts. Experimental Eye Research. 2016; 142: 56–70. https://doi.org/10.1016/j.exer.2015.07.009.

[42] Bandopadhyay S, Mandal S, Ghorai M, Jha NK, Kumar M, Radha, *et al*. Therapeutic properties and pharmacological activities of asiaticoside and madecassoside: A review. Journal of Cellular and Molecular Medicine. 2023; 27: 593–608. https://doi.org/10.1111/jcmm.17635.

[43] Luo W, Bai L, Zhang J, Li Z, Liu Y, Tang X, *et al*. Polysaccharides-based nanocarriers enhance the anti-inflammatory effect of curcumin. Carbohydrate Polymers. 2023; 311: 120718. https://doi.org/10.1016/j.carbpol.2023.120718.